Journal of Materials Chemistry A

PAPER

View Article Online
View Journal | View Issue

Cite this: J. Mater. Chem. A, 2018, 6, 4386

A noble-metal-free nanocatalyst for highly efficient and complete hydrogen evolution from $N_2H_4BH_3$†

Qilu Yao,[a] Zhang-Hui Lu,*[a] Rui Zhang,[b] Shiliang Zhang,[a] Xiangshu Chen*[a] and Hai-Long Jiang[b]

Received 12th December 2017
Accepted 8th February 2018

DOI: 10.1039/c7ta10886a

rsc.li/materials-a

Hydrazine borane ($N_2H_4BH_3$, 15.4 wt% H) has been considered as a highly promising hydrogen storage material because of its inherent advantages such as high hydrogen content and high stability in the solid state. However, the practical application of $N_2H_4BH_3$ for the generation of hydrogen is strongly inhibited by the need for expensive noble metal-based catalysts. To overcome this challenge, noble-metal-free CuNiMo nanocatalysts were prepared using a facile chemical reduction approach under an ambient atmosphere at room temperature. Unexpectedly, the resultant CuNiMo catalyst exhibits excellent catalytic activity, and 100% H_2 selectivity toward hydrogen generation from $N_2H_4BH_3$ *via* its BH_3 group hydrolysis and N_2H_4 moiety decomposition at 323 K. To the best of our knowledge, this is the first report of a noble-metal-free catalyst achieving a complete conversion of $N_2H_4BH_3$ to H_2. In addition, CuNiMo can achieve a complete dehydrogenation of hydrous hydrazine ($N_2H_4{\cdot}H_2O$). The excellent catalytic performance of the $Cu_{0.4}Ni_{0.6}Mo$ catalyst may be attributed to the electronic modification among Cu, Ni and Mo, and may also be related to the strong basic sites of $Cu_{0.4}Ni_{0.6}Mo$. The present simple, low cost, highly efficient, and highly selective catalyst may promote the practical application of $N_2H_4BH_3$ as an effective hydrogen storage material.

1. Introduction

Hydrogen is generally proposed to be a promising efficient energy carrier and an environmentally attractive fuel for future energy application because of its high energy density and efficiency with a low environmental load.[1–5] However, controlled storage and release of hydrogen are the well-known technological barriers in achieving a hydrogen economy society.[6–9] Recently, the chemical storage of hydrogen was considered as an effective solution for practical applications. Among the various types of chemical hydrogen storage materials, ammonia borane (NH_3BH_3) is attractive due to its high hydrogen content (19.6 wt% H).[10–14] Since the mid-2000s, many efforts have been made to achieve the catalytic hydrolysis of NH_3BH_3 (eqn (1)) at room temperature.[10,11] However, the catalytic dehydrogenation of the NH_3 group in NH_3BH_3 is thermodynamically impossible under ambient conditions, which makes the effective gravimetric hydrogen storage capacity (GHSC) of NH_3BH_3–$4H_2O$ decrease to 5.9 wt% H. In recent years, hydrous hydrazine ($N_2H_4{\cdot}H_2O$) has been regarded as a promising liquid-phase hydrogen storage material owing to its high hydrogen content (8.0 wt% H).[15–20] This material could be released by complete decomposition of hydrazine to H_2 and N_2 (eqn (2)), yielding effective GHSC values as high as 8.0 wt% H, although safety issues (*e.g.*, volatility, corrosivity, toxicity, *etc.*) need to be solved for practical application.

$$NH_3BH_3 + 4H_2O \rightarrow NH_4B(OH)_4 + 3H_2 \quad (1)$$

$$N_2H_4 \rightarrow N_2 + 2H_2 \quad (2)$$

$$3N_2H_4 \rightarrow 4NH_3 + N_2 \quad (3)$$

$$N_2H_4BH_3 + 3H_2O \rightarrow N_2H_4 + B(OH)_3 + 3H_2 \quad (4)$$

Hydrazine borane ($N_2H_4BH_3$, 15.4 wt% H), a derivative of NH_3BH_3 where an N_2H_4 group has substituted the NH_3 group, has been regarded as a competitive candidate for chemical hydrogen storage.[21–32] $N_2H_4BH_3$ is also a safe and stable solid material under ambient conditions. This material can be easily prepared by mixing hydrazine hemisulfate and sodium borohydride in dioxane at room temperature.[22] In comparison with the thermolysis of $N_2H_4BH_3$ to release H_2, where high temperature is required and the rate of H_2 generation is low, the catalytic hydrolysis of $N_2H_4BH_3$ can proceed rapidly under mild

[a]Institute of Advanced Materials (IAM), College of Chemistry and Chemical Engineering, Jiangxi Normal University, Nanchang, 330022, P. R. China. E-mail: luzh@jxnu.edu.cn; cxs66cn@jxnu.edu.cn

[b]Hefei National Laboratory for Physical Sciences at the Microscale, Collaborative Innovation Center of Suzhou Nano Science and Technology, Department of Chemistry, University of Science and Technology of China, Hefei, Anhui 230026, P. R. China

† Electronic supplementary information (ESI) available: The detailed experimental procedures, characterization data, and the results of catalytic dehydrogenation of $N_2H_4BH_3$. See DOI: 10.1039/c7ta10886a

conditions.[21,33–37] Like for NH_3BH_3, the BH_3 group in $N_2H_4BH_3$ is readily hydrolyzed in the presence of a suitable catalyst (eqn (4)). The hydrolysis of $N_2H_4BH_3$ was firstly reported by Özkar and co-workers, who only focused on the hydrolysis of the BH_3 group (3 equiv. H_2, eqn (3)).[33] However, unlike the NH_3 moiety of NH_3BH_3, the N_2H_4 moiety in $N_2H_4BH_3$ can also be dehydrogenated to H_2 and N_2 over a selective catalyst (eqn (2)). Hence, $N_2H_4BH_3$ could be ideally dehydrogenated into 5 mol H_2 and 1 mol N_2 per mol NH_3BH_3 in the presence of a selective catalyst. In this case, the effective GHSC of the $N_2H_4BH_3$–$3H_2O$ system reaches 10.0 wt%, which is much higher than those of benchmark hydrogen systems NH_3BH_3–$4H_2O$ (5.9 wt% H)[38–50] and $N_2H_4\cdot H_2O$ (8.0 wt% H).[15–20] The combination of these unique advantages makes $N_2H_4BH_3$ more competitive than the previously widely studied NH_3BH_3 and $N_2H_4\cdot H_2O$.

However, to maximize the usability of $N_2H_4BH_3$ as a hydrogen storage material, the undesired incomplete decomposition to NH_3 (eqn (3)) must be avoided and the catalyst should be economically viable. To this end, extensive efforts have been undertaken to develop an effective catalytic system to realize the selective dehydrogenation of $N_2H_4BH_3$. The first achievement by Demirci and Xu was that 5.79 equivalents of H_2 + N_2 per $N_2H_4BH_3$ were released in the presence of $Ni_{0.89}Pt_{0.11}$ NPs.[24] Although the H_2 selectivity of these catalysts has been greatly improved, the catalytic activities are still too low, mainly due to the sluggish kinetics during the decomposition of the N_2H_4 moiety in $N_2H_4BH_3$. Recent studies have shown that $Ni_{0.6}Pt_{0.4}$/MSC-30 and $Rh_{0.8}Ni_{0.2}$@CeO_x/rGO catalysts can bring about complete conversion of $N_2H_4BH_3$ to H_2 with high activity.[29,30] Despite great progress being made in recent years, all the reported heterogeneous catalysts up to now involve noble metals,[24–32] which greatly limits their large scale practical application due to their high cost and insufficient reserves in the Earth's crust. Therefore, the development of noble-metal-free catalysts with high activity and superior selectivity for complete conversion of $N_2H_4BH_3$ to H_2 is imperative.

Herein, we report a facile approach for synthesizing a noble-metal-free CuNiMo nanocatalyst that shows a favorable catalytic activity, 100% H_2 selectivity, and robust durability for hydrogen generation from $N_2H_4BH_3$ in an alkaline solution, with which 6 equiv. (H_2 + N_2) per $N_2H_4BH_3$ can be released within 13.9 min at 323 K. To the best of our knowledge, this is the first report of a noble-metal-free catalyst achieving the complete conversion of $N_2H_4BH_3$ to H_2 *via* hydrolysis of the BH_3 moiety and decomposition of the N_2H_4 moiety.

2. Experimental

2.1 Chemicals and materials

Hydrazine borane ($N_2H_4BH_3$) was synthesized according to our previously reported procedure.[30–32] Other chemicals were obtained from commercial sources and used without further purification. Copper chloride dihydrate ($CuCl_2\cdot 2H_2O$, Sinopharm Chemical Reagent Co. Ltd., >99%), nickel chloride hexahydrate ($NiCl_2\cdot 6H_2O$, Sinopharm Chemical Reagent Co. Ltd., >98%), cobalt chloride hexahydrate ($CoCl_2\cdot 6H_2O$, Sinopharm Chemical Reagent Co. Ltd., >99%), iron sulfate heptahydrate ($FeSO_4\cdot 6H_2O$, Sinopharm Chemical Reagent Co. Ltd., >99%), sodium molybdate dihydrate ($Na_2MoO_4\cdot 2H_2O$, J&K Scientific Ltd., >99.5%), sodium borohydride ($NaBH_4$, Aldrich, 99%), sodium hydroxide (NaOH, Tianjin Fuchen Chemical Reagent, >96%), and hydrazine monohydrate ($N_2H_4\cdot H_2O$, Aladdin, 98%) were used as received. Ultrapure water with a specific resistance of 18.3 MΩ cm was obtained by reverse osmosis followed by ion exchange and filtration.

2.2 Catalyst characterization

Powder X-ray diffraction (XRD) measurements were carried out on a Rigaku RINT-2000 X-ray diffractometer with a Cu anode, operating at 40 kV and 40 mA. Transmission electron microscopy (TEM, JEM-2010) and scanning transmission electron microscopy (STEM, Titan G2 60-300) coupled with energy dispersive X-ray (EDX) mapping were applied for studying the detailed microstructure of the synthesized samples. The TEM samples were dispersed in ethanol by sonication for 20 min to get a well-dispersed suspension, and one or two droplets of the nanoparticle suspension were dropped onto the amorphous carbon coated copper grid. The chemical compositions of the catalysts were determined using an inductively coupled plasma (ICP) spectrophotometer (Varian, 725-ES). X-ray photoelectron spectroscopy (XPS) was performed after Ar sputtering for 5 min with an ESCALAB MKII X-ray photoelectron spectrometer using monochromatized Al Kα excitation. Temperature programmed desorption of CO_2 (CO_2-TPD) experiments were performed on a Micromeritics AutoChem II 2920 automated apparatus using a thermal conductivity detector (TCD). UV-vis absorption spectra were recorded on a UV-vis spectrophotometer (UV-vis, Hitachi, U-3310). For the UV-Vis measurements, ethanol (25 mL), concentrated hydrochloric acid (2.5 mL, 1 M), and paradimethylaminobenzaldehyde (PDAB, 0.5 g) were mixed together as the chromogenic agent for $N_2H_4BH_3$. Next, 5 mg $N_2H_4BH_3$, 1 mL hydrochloric acid (1 mol L^{-1}), and 50 mL de-ionized water were mixed together as solution A and stored for 12 h before measurements. Then, 0.1 mL of solution A, 2 mL of chromogenic agent, and 25 mL of de-ionized water were mixed, and the sample solutions were stored for 30 min before measurements.

2.3 Preparation of catalysts

2.3.1 Synthesis of the $Cu_{0.4}Ni_{0.6}Mo$ catalyst. The $Cu_{0.4}Ni_{0.6}Mo$ catalyst was synthesized by using a facile one-step reduction method at room temperature. Typically, 6.89 mg of $CuCl_2\cdot 2H_2O$ (0.04 mmol), 14.55 mg of $NiCl_2\cdot 6H_2O$ (0.06 mmol), and 24.45 mg of $Na_2MoO_4\cdot 2H_2O$ (0.1 mmol) were dissolved in 4 mL of water. Then, a 1 mL aqueous solution of $NaBH_4$ (30 mg) was rapidly added into the above solution mixture with vigorous stirring until the bubble generation ceased. Finally, the black product of the $Cu_{0.4}Ni_{0.6}Mo$ catalyst was obtained.

2.3.2 Synthesis of $Cu_{0.4}Ni_{0.6}Mo_x$ catalysts. $Cu_{0.4}Ni_{0.6}Mo_x$ with different molar contents of Mo (x = Mo/(Cu + Ni); x = 0, 0.1, 0.2, 0.4, 0.6, 0.8, 1.0, 1.2, and 1.4) were synthesized using the above method by changing the content of Na_2MoO_4 added, and maintaining the molar content of Cu + Ni at 0.1 mmol.

2.3.3 Synthesis of $Cu_{1-y}Ni_yMo$ catalysts. $Cu_{1-y}Ni_yMo$ NPs with different compositions of Cu and Ni ($y = 0$, 0.2, 0.4, 0.5, 0.6, 0.7, 0.8, and 1.0) were prepared, using a similar method to the one used for preparing the $Cu_{0.4}Ni_{0.6}Mo$ catalyst, by changing the molar contents of Cu and Ni, and maintaining the molar content of Mo at 0.1 mmol.

2.3.4 Synthesis of monometallic Cu, Ni, and Mo catalysts. An analogous synthesis procedure was followed by using only 34.35 mg of $CuCl_2 \cdot 2H_2O$ (0.2 mmol), 48.50 mg of $NiCl_2 \cdot 6H_2O$ (0.2 mmol) or 48.9 mg of $Na_2MoO_4 \cdot 2H_2O$ (0.2 mmol), respectively, for the preparation of monometallic Cu, Ni, and Mo catalysts.

2.3.5 Synthesis of M_1M_2Mo (M_1 and M_2 = Fe, Co, Ni, or Cu) catalysts. M_1M_2Mo (M_1 and M_2 = Fe, Co, Ni, or Cu) nanocatalysts were prepared by using a synthetic methodology similar to that for CuNiMo.

2.4 Catalytic activities for hydrogen generation from $N_2H_4BH_3$

Typically, an aqueous solution (5 mL) containing the $Cu_{0.4}Ni_{0.6}Mo$ catalyst (n_{metal} = 0.2 mmol) and NaOH (2.0 M) was placed in a two-necked round-bottomed flask (50 mL) sealed with a silicon septum. One neck of the flask was connected to a gas burette to measure the volume of the released gas. The reactor was immersed in a water bath to maintain a constant temperature of 323 K. The catalytic reaction started when $N_2H_4BH_3$ (1.0 mmol) was added into the flask with vigorous stirring. The gas released from the reaction was passed through a hydrochloric acid solution (1.0 M) before being measured volumetrically. The reaction was completed when there was no more gas evolved. The selectivity (α) of hydrogen for $N_2H_4BH_3$ dehydrogenation was determined on the basis of the equation $N_2H_4BH_3 + 3H_2O \rightarrow B(OH)_3 + (3 + 2\alpha)H_2 + (2\alpha + 1)/3N_2 + 4(1 - \alpha)/3NH_3$, which can be derived from eqn (2)–(4). Therefore, the selectivity (α) is calculated using the following equation (eqn (5)):

$$\alpha = \frac{3\lambda - 10}{8}\left[\lambda = \frac{n(H_2 + N_2)}{n(N_2H_4BH_3)}\left(\frac{10}{3} \leq \lambda \leq 6\right)\right] \quad (5)$$

The catalytic activities of the other catalysts for hydrogen generation from $N_2H_4BH_3$ were also determined following the above method.

For the durability test, after the catalytic dehydrogenation of $N_2H_4BH_3$ was completed, another equivalent of $N_2H_4BH_3$ (1 mmol) was subsequently added to the flask to initiate the reaction. It should be mentioned that before the durability test, an excess amount of NaOH (5.0 M) was added into the reaction system to neutralize the hydrolysate (H_3BO_3) formed during the first step (the hydrolysis of the BH_3 moiety) of $N_2H_4BH_3$ dehydrogenation.[30,32] These cyclic experiments of the catalysts were repeated 10 times at 323 K.

2.5 Catalytic activities for hydrogen generation from $N_2H_4 \cdot H_2O$

The catalytic activities of $Cu_{0.4}Ni_{0.6}Mo$ NPs for hydrogen generation from $N_2H_4 \cdot H_2O$ (1 mmol) were also determined following the above method for $N_2H_4BH_3$.

3. Results and discussion

3.1 Synthesis and characterization of catalysts

The CuNiMo catalysts were synthesized using a facile one-step approach at room temperature, in which, $CuCl_2 \cdot 2H_2O$, $NiCl_2 \cdot 6H_2O$, and $Na_2MoO_4 \cdot 2H_2O$ were used as the metal precursors and $NaBH_4$ was added as the reducing agent. The as-synthesized CuNiMo catalysts were separated from the reaction solution by centrifugation, washed with water, and dried in a vacuum oven at 313 K. The compositions of the as-synthesized CuNiMo catalysts were determined by inductively coupled plasma atomic emission spectroscopy (ICP-AES). Obviously, the molar ratios of Cu : Ni : Mo are in good agreement with the initial values (Table S1†). Among all the as-synthesized samples, the optimized $Cu_{0.4}Ni_{0.6}Mo$ NPs exhibited the highest activity (*vide infra*), and therefore the $Cu_{0.4}Ni_{0.6}Mo$ catalyst was chosen as the model catalyst for full characterization.

The morphology and size of the as-synthesized $Cu_{0.4}Ni_{0.6}Mo$ NPs were investigated by transmission electron microscopy (TEM). The $Cu_{0.4}Ni_{0.6}Mo$ NPs are well dispersed with a mean particle size of about 5.9 ± 1.2 nm (Fig. 1a and b and S1†). In sharp contrast, without the addition of Mo, the $Cu_{0.4}Ni_{0.6}$ NPs are aggregated to a larger size of about 21.8 ± 5.7 nm (Fig. 1d and S2c†), which clearly demonstrates that the introduction of Mo into $Cu_{0.4}Ni_{0.6}$ NPs can induce the reduction of the metal NP size. In addition, it is found that the size of the $Cu_{0.4}Ni_{0.6}Mo_x$ NPs decreases with increasing the Mo content (Fig. 1 and S2†). High-angle annular dark-field scanning TEM (HAADF-STEM) and elemental mapping images were recorded to examine the distribution of Cu, Ni, and Mo in the Ni–$Cu_{0.4}Ni_{0.6}Mo$ NPs (Fig. 1d). It can be clearly seen that Cu, Ni, and Mo are homogeneously distributed in the metal nanoparticles (Fig. 1c). In

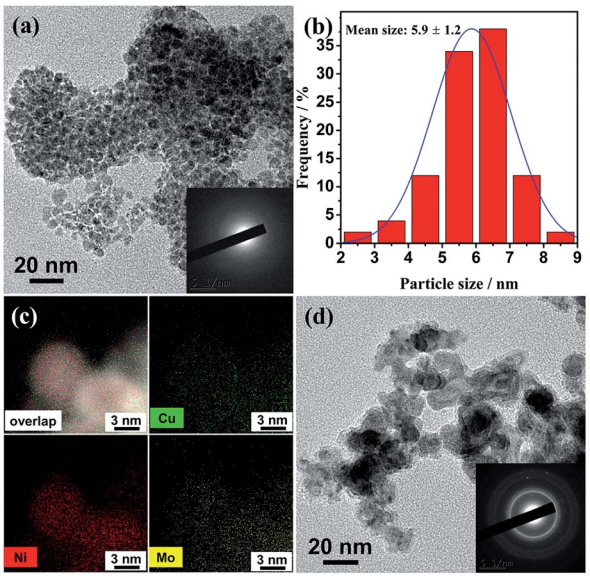

Fig. 1 (a) TEM image and the corresponding SAED pattern, (b) particle size distribution, and (c) HAADF-STEM image and the corresponding elemental mapping images of $Cu_{0.4}Ni_{0.6}Mo$ NPs. (d) TEM image and the corresponding SAED pattern of $Cu_{0.4}Ni_{0.6}$ NPs.

addition, from the selected-area electron diffraction (SAED) patterns, it can be found that the $Cu_{0.4}Ni_{0.6}Mo$ sample is in an amorphous state (Fig. 1a, inset), while the $Cu_{0.4}Ni_{0.6}$ sample is polycrystalline (Fig. 1d, inset), which were further confirmed by high-resolution TEM images (HRTEM, inset of Fig. S2a†) and powder X-ray diffraction (XRD) patterns (Fig. 2, *vide infra*). Therefore, the formation of the amorphous phase of the $Cu_{0.4}Ni_{0.6}Mo$ catalyst may be attributed to the presence of Mo in this sample.

The crystalline structures of the as-synthesized catalysts were further characterized by XRD. As exhibited in Fig. 2, the XRD pattern of $Cu_{0.4}Ni_{0.6}Mo$ shows no obvious diffraction peak (red trace), indicating that the sample is in an amorphous state, which is consistent with its SAED and HRTEM results (inset of Fig. 1a and S1†), while the sample prepared without Mo has an obvious crystalline peak at around $2\theta = 43.64°$ (Fig. 2, blue trace), which is in an intermediate position between the (111) plane of fcc Cu (JCPDS: 04-0836) and the (111) plane of fcc Ni (JCPDS: 04-0850), confirming the alloy structure of $Cu_{0.4}Ni_{0.6}$ NPs. After heat treatment at 873 K for 3 h in an Ar atmosphere, the $Cu_{0.4}Ni_{0.6}Mo$ NP sample is well crystallized. As revealed in Fig. 2 (black trace), the peaks at around $2\theta = 43.70°$, 50.78°, and 74.89° are assigned to the CuNi alloy. The rest of the peaks shown in Fig. 2 (black trace) can be easily indexed to Mo (JCPSD: 65-7442), MoO_2 (JCPSD: 65-5787), and MoO_3 (JCPSD: 05-0508), respectively. Based on the above analyses, it can be concluded that Mo-modified CuNi alloy NPs have been successfully prepared through the present facile chemical reduction method.

X-ray photoelectron spectroscopy (XPS) analyses after Ar sputtering for $Cu_{0.4}Ni_{0.6}Mo$ and $Cu_{0.4}Ni_{0.6}$ NPs were performed to understand the electronic states and surface interaction among Cu, Ni, and Mo. From the XPS spectra, it is apparent that Cu (Fig. 3a) and Ni (Fig. 3b) are present in the metallic state. The Mo species in $Cu_{0.4}Ni_{0.6}Mo$ NPs (Fig. 3c) are found to exist in the form of metallic (Mo, 228.46 eV) and oxidized states (MoO_2, 229.52 eV and MoO_3, 233.41 eV), which is probably due to the fact that it is difficult to reduce Mo ions. In addition, it can be seen that the addition of Mo into $Cu_{0.4}Ni_{0.6}$ NPs results in changes in the binding energy. The binding energies for Cu 2p (Fig. 3a) and Ni 2p (Fig. 3b) in $Cu_{0.4}Ni_{0.6}Mo$ NPs are both shifted to lower binding energies compared with those in $Cu_{0.4}Ni_{0.6}$ NPs, respectively, while the binding energy for metallic Mo in $Cu_{0.4}Ni_{0.6}Mo$ NPs (228.57 eV) is shifted to a higher binding energy compared with that of the standard state of metallic Mo (228.0 eV). These shifts demonstrated that some electrons were transferred from Mo to Cu and Ni in the $Cu_{0.4}Ni_{0.6}Mo$ sample. This modified electronic structure in $Cu_{0.4}Ni_{0.6}Mo$ could have the potential to enhance the catalytic activity for hydrogen generation from $N_2H_4BH_3$. From the CO_2-TPD measurements, we can clearly see that the strength of the basic sites of the $Cu_{0.4}Ni_{0.6}Mo$ NPs is higher than that of the $Cu_{0.4}Ni_{0.6}$ NPs (Fig. 3d and S4†). And the basic sites of the $Cu_{0.4}Ni_{0.6}Mo_x$ NPs tend to gradually strengthen with the increase of Mo content (Fig. S4a†). As strong basic sites are known to be beneficial to the selective cleavage of the N–H bond in the decomposition of N_2H_4 of $N_2H_4BH_3$,[51–56] the $Cu_{0.4}Ni_{0.6}Mo$ NPs may have high selectivity towards the dehydrogenation of $N_2H_4BH_3$ (*vide infra*).

The catalytic performance of the $Cu_{0.4}Ni_{0.6}Mo$ NPs toward the dehydrogenation of $N_2H_4BH_3$ was evaluated in a typical water-filled graduated buret system and compared with that of the Cu, Ni, Mo, $Cu_{0.4}Ni_{0.6}$, CuMo, and NiMo NPs. Remarkably, the $Cu_{0.4}Ni_{0.6}Mo$ NPs exhibited the highest activity among all the catalysts prepared in this work, with which 6.0 equivalents ($H_2 + N_2$) per $N_2H_4BH_3$ (100% selectivity calculated using eqn (5)) can be released within only 13.9 min at 323 K (Fig. 4 and Table S2†). As for the NiMo NPs, 5.1 equivalents of gas can be released within 18.1 min, whereas the CuMo and $Cu_{0.4}Ni_{0.6}Mo$ NPs showed much lower H_2 selectively, with which only 3.3 equivalents of gas were released, respectively. Both monometallic Cu and Ni NPs showed activity for the hydrolysis of the BH_3 group only, and 3.0 equivalents of gas can be generated from the aqueous $N_2H_4BH_3$ solution, respectively (Fig. 4 and

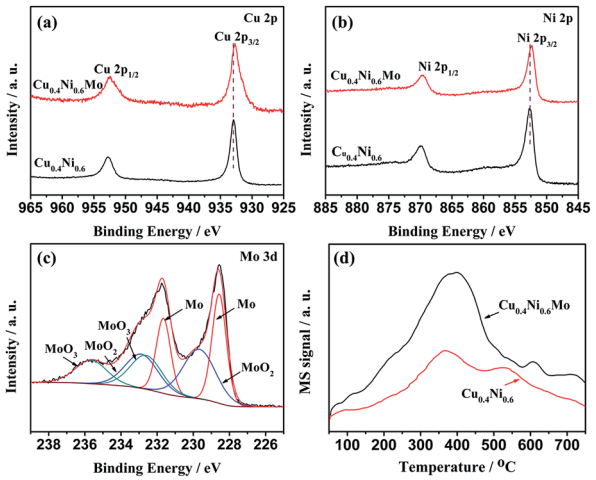

Fig. 3 XPS spectra of (a) Cu 2p, (b) Ni 2p, (c) Mo 3d, and (d) CO_2-TPD mass spectra of the $Cu_{0.4}Ni_{0.6}Mo$ and $Cu_{0.4}Ni_{0.6}$ NPs.

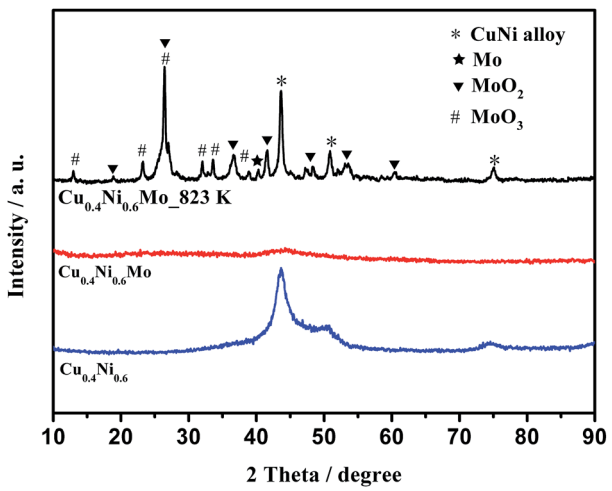

Fig. 2 X-ray diffraction patterns of $Cu_{0.4}Ni_{0.6}$ NPs and $Cu_{0.4}Ni_{0.6}Mo$ NPs before and after heat treatment at 823 K for 3 h under an Ar atmosphere in a tube furnace.

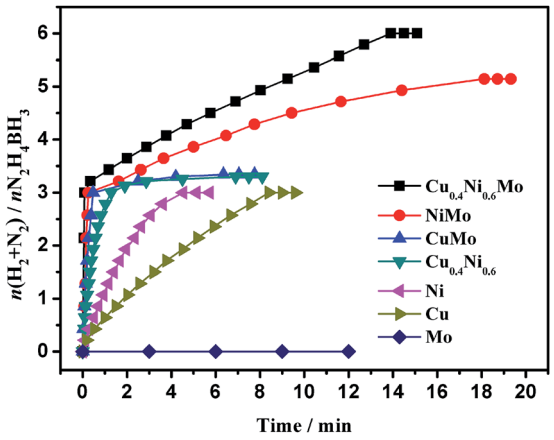

Fig. 4 Time-course plots for the dehydrogenation of $N_2H_4BH_3$ aqueous solution (0.2 M, 5 mL) catalyzed by different catalysts in the presence of NaOH (2.0 M) at 323 K ($n_{metal}/n_{N_2H_4BH_3} = 0.2$).

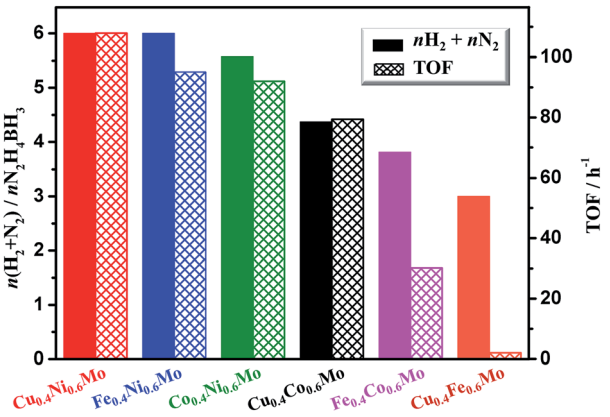

Fig. 5 Catalytic dehydrogenation of $N_2H_4BH_3$ aqueous solution (0.2 M, 5 mL) to generate H_2 over different catalysts in the presence of NaOH (2.0 M) at 323 K ($n_{metal}/n_{N_2H_4BH_3} = 0.2$).

Table S2†). Pure Mo had no catalytic activity, but its presence was clearly found to play an essential role in the synthesis of highly active $Cu_{0.4}Ni_{0.6}Mo_x$ NPs (Fig. S5†). Even adding a small amount of Mo to $Cu_{0.4}Ni_{0.6}$ had a significant effect on the activity and hydrogen selectivity, and the optimal molar ratio, $X_{Mo} = n_{Mo}/n_{(Cu+Ni)}$, was determined to be 1.0. In addition, the catalytic performance of $Cu_{1-y}Ni_yMo$ was also affected by the molar ratio of Cu/Ni. When the molar content of Mo was set at a value of 1.0, the optimum Cu : Ni molar ratio was 0.4 : 0.6 (Fig. S6†). Increasing or decreasing the optimum value can result in the loss of catalytic activity. After catalytic reaction over $Cu_{0.4}Ni_{0.6}Mo$ NPs, the absence of $N_2H_4BH_3$ in the ultraviolet visible (UV-vis) spectrum further confirmed the completeness of the dehydrogenation of $N_2H_4BH_3$ (Fig. S7†). The total turnover frequency (TOF) of $Cu_{0.4}Ni_{0.6}Mo$ was calculated to be 108 h^{-1} at 323 K, a very high value compared to those of reported catalysts (Table S3†).[24–32] To the best of our knowledge, this is the first report of a noble-metal-free catalyst catalyzing the complete dehydrogenation of $N_2H_4BH_3$. The excellent catalytic activities of $Cu_{0.4}Ni_{0.6}Mo$ NPs could be attributed to the electronic modification among Cu, Ni and Mo, and may also be related to the small particle size of $Cu_{0.4}Ni_{0.6}Mo$ NPs. Besides the above-mentioned factors, the strong basic sites of the $Cu_{0.4}Ni_{0.6}Mo$ NPs are another factor contributing to the high activity for the hydrogen generation from the hydrolysis of $N_2H_4BH_3$ (Fig. 3d).

Since the addition of Mo could effectively enhance the activity and selectivity of CuNiMo NPs, other Mo-modified non-noble-metal catalysts were also prepared by the same method as that for CuNiMo NPs, and their catalytic performances for hydrogen generation from $N_2H_4BH_3$ were investigated and compared (Fig. 5, S8–S12, and Table S2†). As shown in Fig. 5, the $Fe_{0.4}Ni_{0.6}Mo$ catalyst also exhibited excellent activities, with which 6.0 equiv. ($H_2 + N_2$) can be released, whereas $Co_{0.4}Ni_{0.6}Mo$ nanoparticles showed 5.6 equiv. ($H_2 + N_2$) for hydrogen generation from $N_2H_4BH_3$ under analogous reaction conditions. In contrast to the high catalytic performance of the Ni-based catalyst, the other catalysts obtained using different non-noble metals (*e.g.*, $Cu_{0.4}Co_{0.6}Mo$) exhibited much lower catalytic activity (4.4 equiv. gases), whereas the $Cu_{0.4}Fe_{0.6}Mo$ catalyst was found to be only active in the hydrolysis of the BH_3 group in $N_2H_4BH_3$ (3.0 equiv. H_2) under our reaction conditions. The above results indicate that the H_2 selectivity of all the Mo-modified non-noble metal catalysts except CuFeMo NPs (Fig. 5) is remarkably improved compared with that of their unmodified counterparts (Fig. S13†).

An alkali was used as an effective promoter for hydrogen generation from $N_2H_4BH_3$ in the presence of the catalyst. As illustrated in Fig. 6, the H_2 selectivity and activity of the

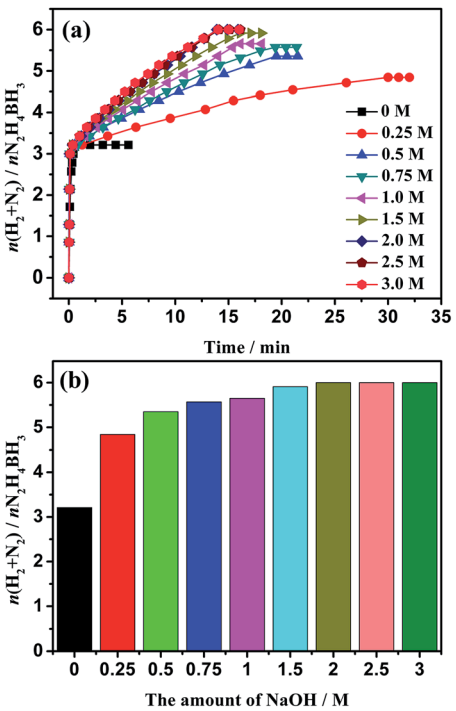

Fig. 6 (a) Time-course plots and (b) NaOH content dependence of $n_{(H_2+N_2)}/n_{(N_2H_4BH_3)}$ for the dehydrogenation of $N_2H_4BH_3$ aqueous solution (0.2 M, 5 mL) catalyzed by $Cu_{0.4}Ni_{0.6}Mo$ NPs with different amounts of NaOH at 323 K ($n_{metal}/n_{N_2H_4BH_3} = 0.2$).

$Cu_{0.4}Ni_{0.6}Mo$ NPs increased rapidly until the concentration of NaOH reached 2.0 M, after which further increasing the NaOH content had no influence on the dehydrogenation of $N_2H_4BH_3$. A possible reason for the promotion effect of alkali can be understood as follows: (a) the existence of OH^- could reduce the amount of undesirable $N_2H_5^+$ ($N_2H_5^+ + OH^- \rightarrow N_2H_4 + H_2O$) in aqueous solution and accelerate the rate-determining deprotonation step ($N_2H_4 \rightarrow N_2H_3^* + H^*$) during the decomposition process of N_2H_4 to H_2 and N_2, and (b) the strong alkaline solution can also help to inhibit the production of NH_3 and thereby raise the H_2 selectivity.[29–32,51–56]

The reaction temperature also greatly affected the catalytic activities. With increasing reaction temperature, the activities of the catalyst were further enhanced (Fig. 7a). Although hydrogen in $N_2H_4BH_3$ can not be completely released with the $Cu_{0.4}Ni_{0.6}Mo$ NPs at room temperature (Fig. 7a), the gas released can reach 5.53 equiv. ($H_2 + N_2$) per $N_2H_4BH_3$. The catalytic reactions for hydrogen generation from $N_2H_4BH_3$ were completed within 37.7, 24.8, 13.9, 8.0, and 3.1 min at 303, 313, 323, 333, and 343 K, respectively, corresponding to TOF values of 37, 59, 108, 187, and 484 h^{-1}. In addition, the increment of reaction rates in each curve (Fig. 7a) showed signs of a slowdown with the increase of time, because the hydrolysis of the BH_3 group (Part 1 in Fig. 7a and S14†) proceeded more quickly and easily than the decomposition of the N_2H_4 group (Part 2 in Fig. 7a) in $N_2H_4BH_3$, consistent with previous reports.[17–25] The values of rate constant k at different temperatures were calculated from the slope of the linear part of each plot in Part 1 and Part 2 from Fig. 7a. According to the Arrhenius plot of ln k *versus* $1/T$, the activation energies of the hydrolysis of the BH_3 group (Part 1) and the decomposition of the N_2H_4 moiety (Part 2) of $N_2H_4BH_3$ are calculated to be 19.8 kJ mol^{-1} (E_{a1}, Fig. 7b) and 54.7 kJ mol^{-1} (E_{a2}, Fig. 7b), respectively. In addition, the activity of the $Cu_{0.4}Ni_{0.6}Mo$ catalyst after heat treatment was also studied. As shown in Fig. S15,† the $Cu_{0.4}Ni_{0.6}Mo$ NPs after heat treatment (at 823 K for 3 h in an Ar atmosphere) showed a lower catalytic activity and selectivity for hydrogen generation from $N_2H_4BH_3$ than those without heat treatment, which is attributed to the fact that $Cu_{0.4}Ni_{0.6}Mo$ NPs tend to sinter into larger species at high temperature as evidenced by TEM observation (12.0 nm, Fig. S16†).

The $Cu_{0.4}Ni_{0.6}Mo$ NPs were also used as a catalyst to decompose the same amount of N_2H_4 as that resulting from the second step of the $N_2H_4BH_3$ dehydrogenation reaction. As shown in Fig. S17a,† the complete decomposition of $N_2H_4 \cdot H_2O$ over $Cu_{0.4}Ni_{0.6}Mo$ NPs at 323 K can finish in 15.5 min with a TOF of 38.7 h^{-1}, which is comparable to those of state-of-the-art catalysts.[15–20,51–56] In addition, the activation energy for the decomposition of $N_2H_4 \cdot H_2O$ was estimated to be 56.6 kJ mol^{-1} (Fig. S17b†), which is higher than that of $Cu_{0.4}Ni_{0.6}Mo$ for the dehydrogenation of the N_2H_4 moiety in $N_2H_4BH_3$ (E_{a2} = 54.7 kJ mol^{-1}). Based on the above results, it can be found that the $Cu_{0.4}Ni_{0.6}Mo$ catalyst showed a lower catalytic activity for hydrogen generation from $N_2H_4 \cdot H_2O$ than that from $N_2H_4BH_3$. A possible explanation is that the rapid hydrolysis of the BH_3 group of $N_2H_4BH_3$ may accelerate the interaction of the resulting N_2H_4 moieties with the $Cu_{0.4}Ni_{0.6}Mo$ catalyst, thus improving the $N_2H_4BH_3$ dehydrogenation kinetics. Similar reaction kinetics were observed in previous studies.[29,30]

Finally, we examined the durability of the $Cu_{0.4}Ni_{0.6}Mo$ catalyst, which is very important for further practical application. The durability test was carried out by successive addition of an additional aliquot of $N_2H_4BH_3$ into the reaction flask when the previous run was completed. As shown in Fig. 8, the catalytic activity of the $Cu_{0.4}Ni_{0.6}Mo$ catalyst is essentially

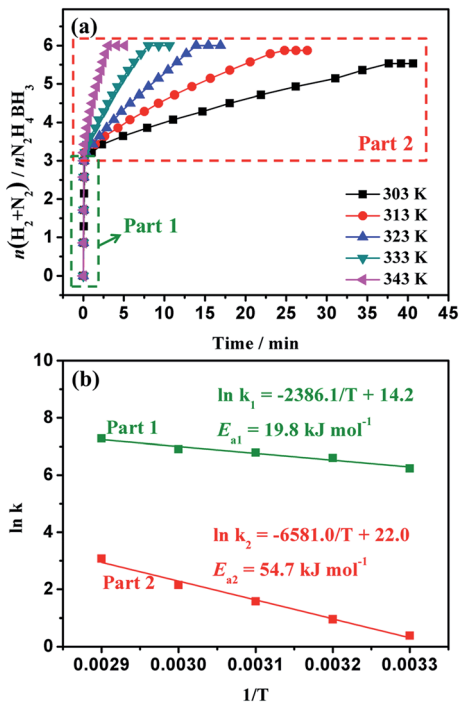

Fig. 7 (a) Time-course plots for the dehydrogenation of $N_2H_4BH_3$ aqueous solution (0.2 M, 5 mL) catalyzed by the $Cu_{0.4}Ni_{0.6}Mo$ catalyst in the presence of NaOH (2.0 M) at different temperatures ($n_{metal}/n_{N_2H_4BH_3}$ = 0.2), and (b) plot of ln k *versus* $1/T$ for hydrogen generation from hydrolysis of the BH_3 group (Part 1) and decomposition of the N_2H_4 moiety of $N_2H_4BH_3$ (Part 2).

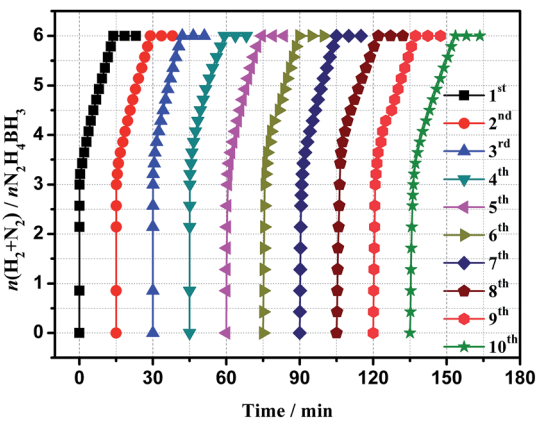

Fig. 8 Durability test for the dehydrogenation of $N_2H_4BH_3$ aqueous solution (0.2 M, 5 mL) catalyzed by $Cu_{0.4}Ni_{0.6}Mo$ NPs with NaOH (5.0 M) at 323 K ($n_{metal}/n_{N_2H_4BH_3}$ = 0.2).

retained even after ten runs, whereas the reaction rate showed a slight decrease. After the durability test, the $Cu_{0.4}Ni_{0.6}Mo$ catalyst was characterized by XRD and TEM techniques. The resulting XRD patterns show an unchanged nanostructure (Fig. S18†), while the TEM image showed an increase of metal size (9.5 nm, Fig. S19†). Thus, the slight decrease in the activity can be ascribed to the increased metal size and the deactivation effect of the increasing metaborate, which accumulates during the hydrolysis of the BH_3 group of $N_2H_4BH_3$.

4. Conclusions

In summary, noble-metal-free CuNiMo catalysts have been facilely prepared *via* a simple *in situ* approach at room temperature under an ambient atmosphere. The optimized $Cu_{0.4}Ni_{0.6}Mo$ catalyst showed excellent catalytic activity and 100% H_2 selectivity for the dehydrogenation of $N_2H_4BH_3$ in an alkaline solution at 323 K. As far as we know, this is the first report of a noble-metal-free catalyst catalyzing the complete dehydrogenation of $N_2H_4BH_3$. In addition, similar FeNiMo, CoNiMo, and CuCoMo catalysts also show good activity for hydrogen evolution from $N_2H_4BH_3$. This remarkable improvement of the catalytic performance of noble-metal-free heterogeneous catalysts demonstrates a promising strategy towards the development of $N_2H_4BH_3$ as a feasible chemical hydrogen storage material for application in fuel cells.

Conflicts of interest

There are no conflicts to declare.

Acknowledgements

This work was financially supported by the National Natural Science Foundation of China (21763012, 21463012, 21371162, 21673213, and 21521001), the Natural Science Foundation of Jiangxi Province of China (20171ACB21021 and 2016BAB203087) and the National Research Fund for Fundamental Key Project (2014CB931803).

Notes and references

1 P. Chen, Z. Xiong, J. Luo, J. Lin and K. L. Tan, *Nature*, 2002, **420**, 302–304.
2 H. L. Jiang, S. K. Singh, J. M. Yan, X. B. Zhang and Q. Xu, *ChemSusChem*, 2010, **3**, 541–549.
3 Z. L. Wang, J. M. Yan, Y. Ping, H. L. Wang, W. T. Zheng and Q. Jiang, *Angew. Chem., Int. Ed.*, 2013, **52**, 4406–4409.
4 Q. Y. Bi, X. L. Du, Y. M. Liu, Y. Cao, H. Y. He and K. N. Fan, *J. Am. Chem. Soc.*, 2012, **134**, 8926–8933.
5 X. Xia, L. Cosme-Figueroa, J. Tao, H. C. Peng, G. Niu, Y. Zhu and Y. Xia, *J. Am. Chem. Soc.*, 2014, **136**, 10878–10881.
6 C. W. Hamilton, R. T. Baker, A. Staubitz and I. Manners, *Chem. Soc. Rev.*, 2009, **38**, 279–293.
7 Y. Huang, X. Zhou, M. Yin, C. Liu and W. Xing, *Chem. Mater.*, 2010, **22**, 5122–5128.
8 M. Yadav and Q. Xu, *Energy Environ. Sci.*, 2012, **5**, 9698–9725.
9 Q. L. Zhu and Q. Xu, *Energy Environ. Sci.*, 2015, **8**, 478–512.
10 M. Chandra and Q. Xu, *J. Power Sources*, 2006, **156**, 190–194.
11 W. W. Zhan, Q. L. Zhu and Q. Xu, *ACS Catal.*, 2016, **6**, 6892–6905.
12 H. Yan, Y. Lin, H. Wu, W. Zhang, Z. Sun, H. Cheng, W. Liu, C. Wang, J. Li, X. Huang, T. Yao, J. Yang, S. Wei and J. Lu, *Nat. Commun.*, 2017, **8**, 1070.
13 C. C. Hou, Q. Li, C. J. Wang, C. Y. Peng, Q. Q. Chen, H. F. Ye, W. F. Fu, C. M. Che, N. López and Y. Chen, *Energy Environ. Sci.*, 2017, **10**, 1770–1776.
14 L. Zhou, J. Meng, P. Li, Z. Tao, L. Mai and J. Chen, *Mater. Horiz.*, 2017, **4**, 268–273.
15 S. K. Singh and Q. Xu, *J. Am. Chem. Soc.*, 2009, **131**, 18032–18033.
16 J. Wang, X. B. Zhang, Z. L. Wang, L. M. Wang and Y. Zhang, *Energy Environ. Sci.*, 2012, **5**, 6885–6888.
17 L. He, Y. Huang, A. Wang, X. Wang, X. Chen, J. J. Delgado and T. Zhang, *Angew. Chem., Int. Ed.*, 2012, **51**, 6191–6194.
18 S. K. Singh and Q. Xu, *Catal. Sci. Technol.*, 2013, **3**, 1889–1900.
19 Z. Zhang, S. Zhang, Q. Yao, X. Chen and Z. H. Lu, *Inorg. Chem.*, 2017, **56**, 11938–11945.
20 W. Kang and A. Varma, *Appl. Catal., B*, 2018, **220**, 409–416.
21 T. Hügle, M. F. Kühnel and D. Lentz, *J. Am. Chem. Soc.*, 2009, **131**, 7444–7447.
22 R. Moury, G. Moussa, U. B. Demirci, J. Hannauer, S. Bernard, E. Petit, A. V. D. Lee and P. Miele, *Phys. Chem. Chem. Phys.*, 2012, **14**, 1768–1777.
23 T. He, H. Wu, G. Wu, J. Wang, W. Zhou, Z. Xiong, J. Chen, T. Zhang and P. Chen, *Energy Environ. Sci.*, 2012, **5**, 5686–5689.
24 J. Hannauer, O. Akdim, U. B. Demirci, C. Geantet, J. M. Herrmann, P. Miele and Q. Xu, *Energy Environ. Sci.*, 2011, **4**, 3355–3358.
25 D. C. Zhong, K. Aranishi, A. K. Singh, U. B. Demirci and Q. Xu, *Chem. Commun.*, 2012, **48**, 11945–11947.
26 Ç. Çakanyıldırım, U. B. Demirci, T. Şener, Q. Xu and P. Miele, *Int. J. Hydrogen Energy*, 2012, **37**, 9722–9729.
27 D. Clémençon, J. F. Petit, U. B. Demirci, Q. Xu and P. Miele, *J. Power Sources*, 2014, **260**, 77–81.
28 C. Li, Y. Dou, J. Liu, Y. Chen, S. He, M. Wei, D. G. Evans and X. Duan, *Chem. Commun.*, 2013, **49**, 9992–9994.
29 Q. L. Zhu, D. C. Zhong, U. B. Demirci and Q. Xu, *ACS Catal.*, 2014, **4**, 4261–4268.
30 Z. J. Zhang, Z. H. Lu, H. L. Tan, X. S. Chen and Q. L. Yao, *J. Mater. Chem. A*, 2015, **3**, 23520–23529.
31 Z. J. Zhang, Z. H. Lu and X. S. Chen, *ACS Sustainable Chem. Eng.*, 2015, **3**, 1255–1261.
32 Z. J. Zhang, Y. Q. Wang, X. S. Chen and Z. H. Lu, *J. Power Sources*, 2015, **291**, 14–19.
33 S. Karahan, M. Zahmakıran and S. Özkar, *Int. J. Hydrogen Energy*, 2011, **36**, 4958–4966.
34 Q. L. Yao, Z. H. Lu, Z. J. Zhang, X. S. Chen and Y. Q. Lan, *Sci. Rep.*, 2014, **4**, 7597.
35 Q. L. Yao, Z. H. Lu, K. K. Yang, X. S. Chen and M. H. Zhu, *Sci. Rep.*, 2015, **5**, 15186.

36 D. Özhava, N. Z. Kılıçaslan and S. Özkar, *Appl. Catal., B*, 2015, **162**, 573–582.
37 K. K. Yang, Q. L. Yao, W. Huang, X. S. Chen and Z. H. Lu, *Int. J. Hydrogen Energy*, 2017, **42**, 6840–6850.
38 P. Pachfule, X. Yang, Q. L. Zhu, N. Tsumori, T. Uchida and Q. Xu, *J. Mater. Chem. A*, 2017, **5**, 4835–4841.
39 H. Zhang, X. J. Gu, P. L. Liu, J. Song, J. Cheng and H. Q. Su, *J. Mater. Chem. A*, 2017, **5**, 2288–2296.
40 J. M. Yan, X. B. Zhang, T. Akita, M. Haruta and Q. Xu, *J. Am. Chem. Soc.*, 2010, **132**, 5326–5327.
41 X. Wang, D. Liu, S. Song and H. Zhang, *J. Am. Chem. Soc.*, 2013, **135**, 15864–15872.
42 W. Chen, J. Ji, X. Feng, X. Duan, G. Qian, P. Li, X. Zhou, D. Chen and W. Yuan, *J. Am. Chem. Soc.*, 2014, **136**, 16736–16739.
43 J. X. Kang, T. W. Chen, D. F. Zhang and L. Guo, *Nano energy*, 2016, **23**, 145–152.
44 M. A. Khalily, H. Eren, S. Akbayrak, H. H. Susapto, N. Biyikli, S. Özkar and M. O. Guler, *Angew. Chem., Int. Ed.*, 2016, **55**, 12257–12261.
45 Ö. Metin, V. Mazumder, S. Özkar and S. Sun, *J. Am. Chem. Soc.*, 2010, **132**, 1468–1469.
46 Y. Z. Chen, Q. Xu, S. H. Yu and H. L. Jiang, *Small*, 2015, **11**, 71.
47 C. Y. Peng, L. Kang, S. Cao, Y. Chen, Z. S. Lin and W. F. Fu, *Angew. Chem., Int. Ed.*, 2015, **54**, 15725–15729.
48 K. Feng, J. Zhong, B. Zhao, H. Zhang, L. Xu, X. Sun and S. T. Lee, *Angew. Chem., Int. Ed.*, 2016, **55**, 11950–11954.
49 Q. L. Yao, Z. H. Lu, W. Huang, X. Chen and J. Zhu, *J. Mater. Chem. A*, 2016, **4**, 8579–8583.
50 Z. Li, T. He, L. Liu, W. Chen, M. Zhang, G. Wu and P. Chen, *Chem. Sci.*, 2017, **8**, 781–788.
51 S. K. Singh, A. K. Singh, K. Aranishi and Q. Xu, *J. Am. Chem. Soc.*, 2011, **133**, 19638–19641.
52 L. He, Y. Huang, A. Wang, X. Wang and T. Zhang, *AIChE J.*, 2013, **59**, 4297–4302.
53 J. Zhang, Q. Kang, Z. Yang, H. Dai, D. Zhuang and P. Wang, *J. Mater. Chem. A*, 2013, **1**, 11623–11628.
54 J. Wang, Y. Li and Y. Zhang, *Adv. Funct. Mater.*, 2014, **24**, 7073–7077.
55 H. L. Wang, J. M. Yan, S. J. Li, X. W. Zhang and Q. Jiang, *J. Mater. Chem. A*, 2015, **3**, 121–124.
56 J. Wang, W. Li, Y. Wen, L. Gu and Y. Zhang, *Adv. Energy Mater.*, 2015, 1401879.